Asian Journal of Chemistry; Vol. 34, No. 4 (2022), 995-1002

ASIAN JOURNAL OF CHEMISTRY

https://doi.org/10.14233/ajchem.2022.23547

Synthesis of Novel Ionic Liquid Modified AC-Fe_3O_4 Magnetic Nanocomposite for the Adsorption of Heavy Metals in Wastewater

R.T. TAZIWA, H. MUNGONDORI* and TAKUNDA ZARIMA

Department of Applied Chemistry, Walter Sisulu University, Old King Williams Road, Fort Jackson, East London, South Africa

*Corresponding author: Tel: +27 60 5038175; E-mail: henrymungondori@gmail.com

Received: 25 September 2021; *Accepted*: 1 February 2022; *Published online*: 10 March 2022; AJC-20745

This study reports a novel magnetic nanoadsorbent prepared from magnetite (Fe_3O_4) as the magnetic core, activated carbon from coal fly ash and an ionic liquid (1-methyl-3-ethylimidazolium chloride). The magnetic nanoadsorbent was synthesized *via* co-precipitation and characterized by FTIR, XRD, TEM, EDS and BET surface area analysis. Batch adsorption studies on cadmium (Cd^{2+}) and lead (Pb^{2+}) solutions such as effect of pH, contact time and adsorbent dosage were carried out. The data was analyzed using the Langmuir and Freundlich models. The results revealed that the optimal adsorption conditions for both metal ions on synthesized nanoadsorbent were pH 6, 200 min, adsorbent dosage of 1.5 g/L, initial ion concentration of 10 ppm and a temperature of 25 ºC. The data obtained in the adsorption of Cd^{2+} and Pb^{2+} best fitted the Freundlich isotherm, with R^2 values of 0.998 and 0.995, respectively. Thermodynamic and kinetic studies suggested that adsorption of both metal ions on the IL-AC-Fe_3O_4 nanocomposite followed the pseudo first order model. The synthesised nanoadsorbent (IL-AC-Fe_3O_4) exhibits good adsorption properties and has great potential in a water treatment technology.

Keywords: Adsorption, Heavy metals, Lead, Cadmium, Nanoadsorbent, Wastewater.

INTRODUCTION

Environmental heavy metal pollution is one of the negative effects of rapid industrialization. Continuous discharge of effluent from industries such as metal processing refineries, coal powered electricity generating plants, paper processing, textiles, *etc*. into water bodies has led to the rapid deterioration of water quality, making it unsuitable for human consumption without further purification [1,2]. Heavy metals are known to cause several health problems in human beings, some of which can lead to death [3,4]. Cadmium and lead are among the most frequently encountered toxic heavy metals. When discarded in wastewater, these metals can cause a serious harm to the aquatic life [5,6]. Cadmium is persistent and cannot be broken down into less toxic chemical substances in the environment. Due to its higher thiophilicity, Cd^{2+} has been observed to replace Zn^{2+} in zinc enzymes, leading to their deactivation in most living organisms. A similar trend is observed in bones where it replaces Ca^{2+}, leading to porosity and weakening [7]. It is apparent that researchers have to do more to allow the supply of potable water worldwide.

Water treatment methods that are currently in use for the removal of heavy metals include membrane separation, filtration, electrochemistry, adsorption, chemical precipitation, solvent extraction and ion exchange [8,9]. These methods have their own advantages and disadvantages. Owing to its simplicity and effectiveness, adsorption has been considered a method of choice in the removal of heavy metals in water [10]. The current water supply challenges such emergence of new recalcitrant pollutants have prompted researchers to develop new methods, which offer high efficiency, multi-functionality and flexibility in system size. In order to develop highly efficient adsorbents, researchers have focused their attention on nano-scale adsorbents referred to as nanoadsorbents. The small size offers high surface area, which increases sorption capacity [11]. Reduction in size comes with separation challenges and these have led researchers to develop magnetic nanoadsorbents.

Most of the magnetic nanoadsorbents are based on magnetite owing to its high saturation magnetization and high surface area. However, synthetic magnetite easily oxidizes to maghemite or hematite if it comes in contact with atmospheric or water dissolved oxygen, leading to a drop in saturation magnetization

[12]. In a bid to produce magnetic nanoadsorbents with a balance in magnetic properties and adsorption capacity, Campos *et al.* [11] reported core-shell bimagnetic nanoparticles as novel adsorbent for Cr(VI) removal from water. The nanoadsorents showed good selectivity for Cr(VI) adsorption. In another study, an amino/thio bifunctionalized nanoadsorbent was employed in the removal of Pb(II) from an aqueous environment. A dramatic increase in adsorption was observed owing to the synergistic effects of the -NH_2 and -SH groups [8].

In this study, a novel magnetic nanoadsorbent was prepared from magnetite (Fe_3O_4) as the magnetic core and coupled with activated carbon from coal fly ash. The resulting nanocomposite was then modified with an ionic liquid (1-methyl-3-ethylimidazolium chloride) to enhance the adsorption capacity. The study explored the effect of pH, contact time, adsorbent dosage, initial heavy metal ion concentration and temperature on the adsorption process.

EXPERIMENTAL

The materials *viz*. iron(II) chloride tetrahydrate ($FeCl_2 \cdot 4H_2O$) (98%, Merck), iron(III) chloride hexahydrate ($FeCl_3 \cdot 6H_2O$) (99%, Merck), methanol (99.9%, Merck), 1-ethyl-3-methylimidazolium chloride [EMIM]Cl (98%, Merck), nitrogen gas (Linde), cadmium nitrate (98%, Merck) and lead nitrate (99%, HiMedia laboratories Pvt. Ltd.) and coal fly ash (CFA) (Eskom power plant, South Africa) were obtained and used as such without further purification.

General procedure: Magnetite (Fe_3O_4) nanoparticles were synthesized using a chemical co-precipitation method where ferric chloride ($FeCl_3 \cdot 6H_2O$) and ferrous chloride ($FeCl_2 \cdot 4H_2O$) salts were dissolved with a ratio of 2.6:1, respectively in 200 mL of deoxygenated distilled water under a N_2 atmosphere [13]. After 1 h of mechanical stirring, chemical precipitation was achieved at 30 ºC by the addition of 2 M NaOH solution in a N_2 environment. Reaction system was maintained at 70 ºC for 5 h with a pH of 12 to allow complete precipitation. After cooling the system to room temperature, the precipitate was isolated through the use of a permanent magnet and then washed with deoxygenated distilled water until neutral pH was attained. Acetone was used to wash Fe_3O_4 nanoparticles before drying in an oven around 60 ºC.

AC-Fe_3O_4 magnetic nanoparticles (MNPs) were prepared according to a method in literature [14], using as synthesized Fe_3O_4 MNPs and activated carbon obtained form coal fly ash (CFA). The CFA powder (dried in an oven with the temperature set at 105 ºC for 24 h to expel any moisture present) was impregnated with nitric acid (63%) for 3 h at 80 ºC under ultrasonication. The sample was then filtered and dried at room temperature. A 5 g sample of the dried powder was then dispersed into 200 mL of an aqueous solution containing $Fe_3O_4 \cdot 9H_2O$ and ultrasonicated for an hour at 80 ºC. The sample was then filtered and dehydrated in an oven at about 105 ºC for 1 h, followed by heat treatment in a furnace for 3 h at 750 ºC. The product was then washed with deionized water four times and subsequently dried at 105 ºC.

The AC-Fe_3O_4 MNPs (5 g) were first dispersed into 100 mL of methanol by sonication for about 0.5 h for homogeni-zation. 1-Ethyl-3-methylimidazolium chloride (1 g, 10.6 mmol) was then added with continuous stirring at 60 ºC for 24 h. The reaction mixture was then filtered and Soxhlet extraction carried out for 10 h using acetone. The product was then washed with deionized water and dried in oven at 60 ºC.

Detection method: A Perkin-Elmer Spectrum two Fourier transform infrared (FTIR) spectrometer was used to identify the functional groups present in the prepared materials (Fe_3O_4, AC-Fe_3O_4 and IL-AC-Fe_3O_4 MNPs). Identification of the crystal phases and estimation of particle sizes was carried out on a Bruker-AXS D8 Advance diffractometer (CuKα radiation with a wavelength of 1.5406 Å) comprising of a PSD Lynx-Eye Si-strip detector at room temperature. A Micromeritics Pulse Chemisorb 2700 nitrogen adsorption apparatus was used for the analysis of Brunauer-Emmett-Teller (BET) surface area and pore diameter measurements for the prepared nanoparticles. Micrographs of the AC-Fe_3O_4 magnetic nanoparticles were recorded on a JEM 200CX transmission electron microscope (TEM). Elemental composition was determined using a TESCAN VEGA 3 energy dispersive X-ray spectrometer (EDS).

Batch studies: Batch absorption studies were carried out to evaluate the adsorption capacity of the IL-AC-Fe_3O_4 MNPs adsorbent in the removal of Cd^{2+} and Pb^{2+} ions from aqueous solutions. All the experiments were carried out in triplicate using 250 mL Erlenmeyer flask. The process involved agitation of a given dose of the adsorbent. A 0.1 g sample of adsorbent was dispersed in 100 mL of synthetic heavy metal ion solution at 25 ºC. The prepared mixtures were placed on a rotary shaker and agitated at 220 rpm for 5 h. Aliquots of the sample solution were collected at set time intervals and concentration determined by atomic absorption spectroscopy. A hand-held permanent magnet was used to allow separation of adsorbent from solution (Fig. 1). The effects of temperature, pH, initial heavy metal pollutant concentration, adsorbent dose and contact time were investigated to establish how they influence the adsorption process. The adsorbed amounts (mg g^{-1}) of Cd^{2+} and Pb^{2+} at equilibrium (q_e) were calculated as follows:

$$q_e = \frac{C_o - C_e}{w} \quad (1)$$

Also, the percentage removal efficiency was calculated using the eqn. 2:

$$\text{Removal } (\%) = \frac{C_o - C_e}{C_o} \times 100 \quad (2)$$

Fig. 1. Magnetic separation of nanoadsorbent from treated water

where C_o and C_e are initial and equilibrium concentrations (ppm) of Cd^{2+} and Pb^{2+}; w is the nanoadsorbent concentration (g/L).

Batch tests were also carried out in the temperature range 20-80 ºC to investigate the thermodynamics of the adsorption process. To evaluate the pH dependence of adsorption process, batch experiments were carried out with 100 mL solutions of Cd^{2+} and Pb^{2+} (100 ppm) at different pH values (2, 4, 6, 8, 10). The pH was adjusted using either 0.1 M HCl or 0.1 M NaOH and contact time was 5 h at 25 ºC.

Adsorption kinetics were evaluated by varying contact time between nanoadsorbent and heavy metal pollutant from 0 to 5 h. The nanoadsorbent dose was 0.1 g in 100 mL solutions at pH 6 and a temperature of 25 ºC. To analyze the experimental data, the pseudo first-order and the pseudo second-order kinetic models were used (eqns 3 and 4):

Pseudo first-order kinetics model:

$$\ln (Q_e - Q_t) = \ln Q_e - (k_1)t \quad (3)$$

Pseudo second-order kinetics model:

$$\frac{t}{Q_t} = \frac{1}{k_2 Q_e^2} + \frac{t}{Q_e} \quad (4)$$

where Q_e and Q_t (mg/g) are the amount of heavy metal ions adsorbed at equilibrium and at time t (min), respectively; k_1 (min^{-1}) and k_2 (g $mg^{-1}min^{-1}$) are rate constants of the first-order and second-order adsorption kinetics, respectively.

The adsorption isotherms were acquired by varying the concentration of Cd^{2+} and Pb^{2+} solutions in the range 10 to 100 ppm at 25 ºC and pH 6. The experimental data were fitted into the Freundlich and Langmuir isotherm models for analysis. The Freundlich isotherm is based on the postulation that the adsorption process will take place on heterogeneous surfaces of adsorbent with non-uniform distribution of adsorption heat, whereas the Langmuir isotherm postulates that the adsorption process occurs on homogenous sorbent surfaces with constant energy. The equations for the models are as follows:

Freundlich equation:

$$\ln Q_e = \ln K_f + \frac{1}{n} \ln C_e \quad (5)$$

Langmuir equation:

$$\frac{C_e}{Q_e} = \frac{1}{bQ_o} + \frac{C_e}{Q_o} \quad (6)$$

where C_e (ppm) is the equilibrium concentration of the heavy metals in the liquid phase, Q_e (mg/g) is the solid phase equilibrium concentration of heavy metals, Q_o is the Langmuir monolayer sorption capacity, b (L/mg) is the Langmuir equilibrium adsorption constant and K_f and n are the Freundlich equilibrium adsorption constants.

The Gibbs free energy change (ΔG^o) can be used to assess the spontaneity of an adsorption process. The Gibbs free energy is calculated using equilibrium conditions as follows:

$$\Delta G^\circ = -RT \ln K \quad (7)$$

where R (8.314 J $K^{-1}mol^{-1}$) is universal gas constant, T (K) is the solution temperature and K is the thermodynamic equilibrium constant. The other two thermodynamic parameters, standard enthalpy and entropy (ΔH^o and ΔS^o) were calculated from the van't Hoff equation:

$$\ln K = \frac{\Delta H^\circ}{RT} + \frac{\Delta S^\circ}{R} \quad (8)$$

from the slope and intercept of the plots of ln K *versus* 1/T, respectively [15].

RESULTS AND DISCUSSION

FTIR studies: Fourier transform infrared spectroscopy (FTIR) was used to reveal the functional groups present on the prepared nanoadsorbent material (Fig. 2). In the three spectra, the common peaks are the broad peak centred at 3370 cm^{-1} and 1636 cm^{-1}, attributed to O-H stretching vibrations and bending vibrations for adsorbed water respectively. The peak at 550 cm^{-1} ascribed to Fe-O stretching vibrations [16]. In the spectrum for IL-AC-Fe_3O_4 (Fig. 2c), the bands at 3089 and 2982 cm^{-1} are ascribed to aromatic -C-H and aliphatic -C-H bond vibrations, respectively. The peak at 2867 cm^{-1} is attributed to the N-H bond. The bands occurring at 1565, 1452, 1335 and 1166 cm^{-1} are ascribed to ring stretching symmetries. The short peak at 1090 cm^{-1} is related to the -C-H ring structure in-plane bending vibrations [17].

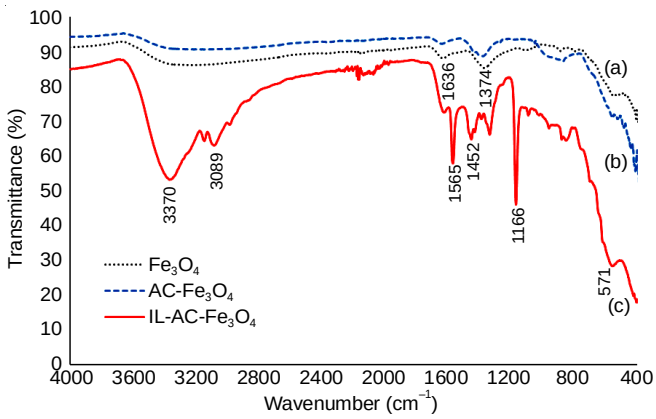

Fig. 2. FTIR spectra of (a) Fe_3O_4, (b) AC-Fe_3O_4 and (c) IL-AC-Fe_3O_4

XRD studies: X-ray diffraction (XRD) analysis was used to study the crystal structure of the magnetic nanoadsorbent as well as estimate particle sizes (Fig. 3). Patterns for Fe_3O_4, AC-Fe_3O_4 and IL-AC-Fe_3O_4 were recorded in the 2θ range 15 to 80º at 25 ºC using CuKα radiation (λ = 1.5406 Å).

The XRD patterns obtained exhibited peaks at 2θ angles of 30.6º, 35.3º, 57.8º, 62.6º, 74.2º and 74.9º corresponding to the 220, 311, 511, 440, 533 and 622 planes according to the Joint Committee on Powder Diffraction Standards (JCPDS) card No. 00-019-0629. The magnetic nanoparticles were confirmed to have face centred cubic arrangement (2θ = 35.3º) [18]. The patterns also exhibited sharp intense peaks at 31.5º and 45.4º belonging to halite, which caused diminishing of the magnetite peaks. The patterns of AC-Fe_3O_4 and IL-AC-Fe_3O_4 revealed the presence of Akaganeite-M [FeO(OH)] and iron oxide hydroxide [FeO(OH)] at 2θ angles of 27.0º and 27.4º, respectively. Iron oxide hydroxide is the product of reaction between an Fe(III) salt with sodium hydroxide.

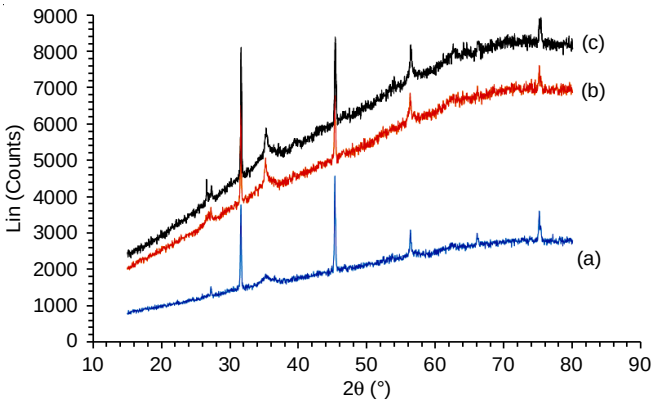

Fig. 3. XRD patterns for (a) Fe_3O_4, (b) IL-AC-Fe_3O_4 and (c) AC-Fe_3O_4

TEM studies: TEM analysis was used to study the morphology of the prepared nanoadsorbent materials (Fig. 4). The micrograph of Fe_3O_4 (Fig. 4a) shows particles which look roughly cube shaped, while that of AC-Fe_3O_4 (Fig. 4b) shows dark spots of Fe_3O_4 nanoparticles embedded in the activated carbon (grey areas). The IL-AC-Fe_3O_4 nanoadsorbent particles (Fig. 4c) were slightly bigger which is consisted with the synthesis process which starts with a magnetic core coated activated carbon then modified with a layer of ionic liquid to enhance the adsorption properties. The average TEM particle sizes were 7.14, 11.90 and 16.67 nm for Fe_3O_4, AC-Fe_3O_4 and IL-AC-Fe_3O_4, respectively, which was consistent with BET surface area (Table-1), where a slight decrease in surface was observed from Fe_3O_4 to IL-AC-Fe_3O_4 with growth in particle size.

TABLE-1
BET SURFACE AREA AND PORE VOLUME
FOR Fe_3O_4, AC-Fe_3O_4 AND IL-AC-Fe_3O_4

Sample	Surface area (BET) (m^2/g)	Pore volume (cm^3/g)
Fe_3O_4	62.7844	0.09167
AC-Fe_3O_4	60.5033	0.11806
IL-AC-Fe_3O_4	57.4049	0.13414

The reduction in BET surface area for the IL-AC-Fe_3O_4 can be attributed to the presence of Fe_3O_4 on the structure of the activated carbon blocking the AC pores [19].

EDX studies: Energy dispersive X-ray spectroscopy (EDX) was used to study the elemental composition of the prepared nanoadsorbent materials. The EDX spectrum of IL-AC-Fe_3O_4 (Fig. 5c) confirmed the presence of the elements Fe and O, which are attributed to magnetite and the elements C, N and Cl, which are the constituents of activated carbon and ionic liquid (1-ethyl-3-methylimidazolium chloride). The findings are in agreement with FTIR analysis which confirmed the functional groups present as well as XRD which confirmed the crystal phases of magnetite.

Optimized parameters

Effect of pH: To evaluate the effects of temperature and pH on adsorption, the removal efficiencies for Cd^{2+} and Pb^{2+} were calculated in relation to changes in temperature and pH (Fig. 6). The findings revealed a sharp increase in the removal efficiencies with increasing pH up to an optimum pH of 6. Removal efficiencies of 99.3 and 90.0% were achieved for

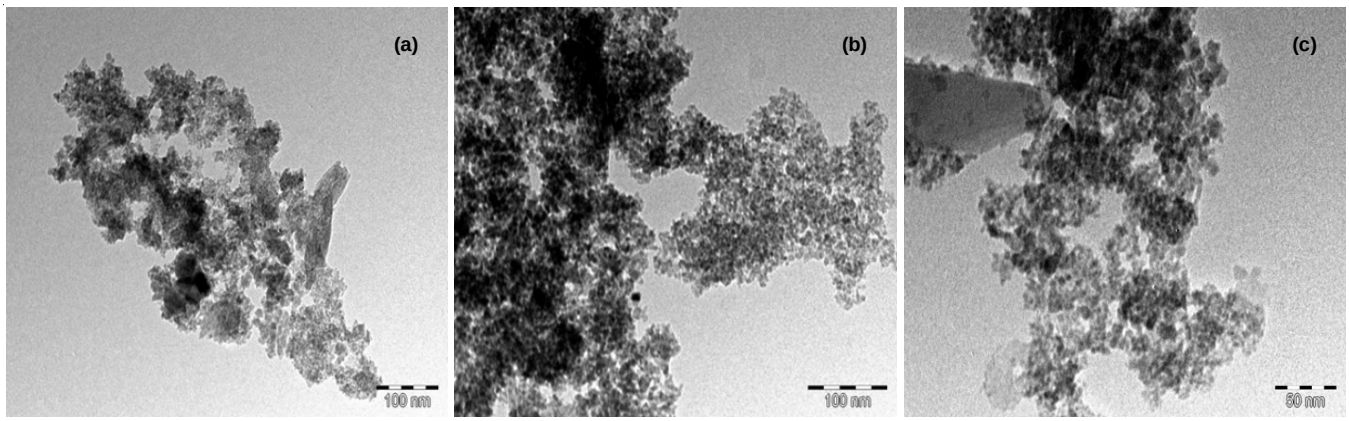

Fig. 4. TEM images of (a) Fe_3O_4, (b) AC-Fe_3O_4 and (c) IL-AC-Fe_3O_4

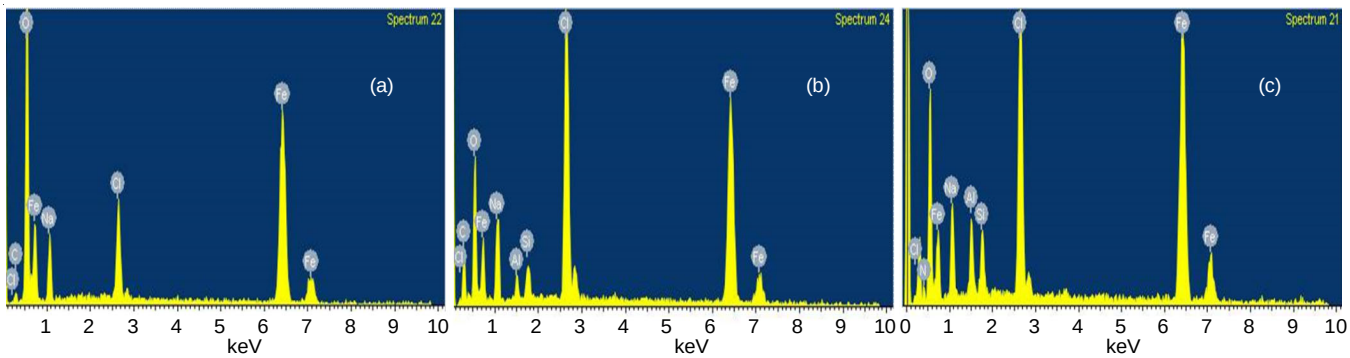

Fig. 5. EDX spectra for (a) Fe_3O_4, (b) AC-Fe_3O_4 and (c) IL-AC-Fe_3O_4

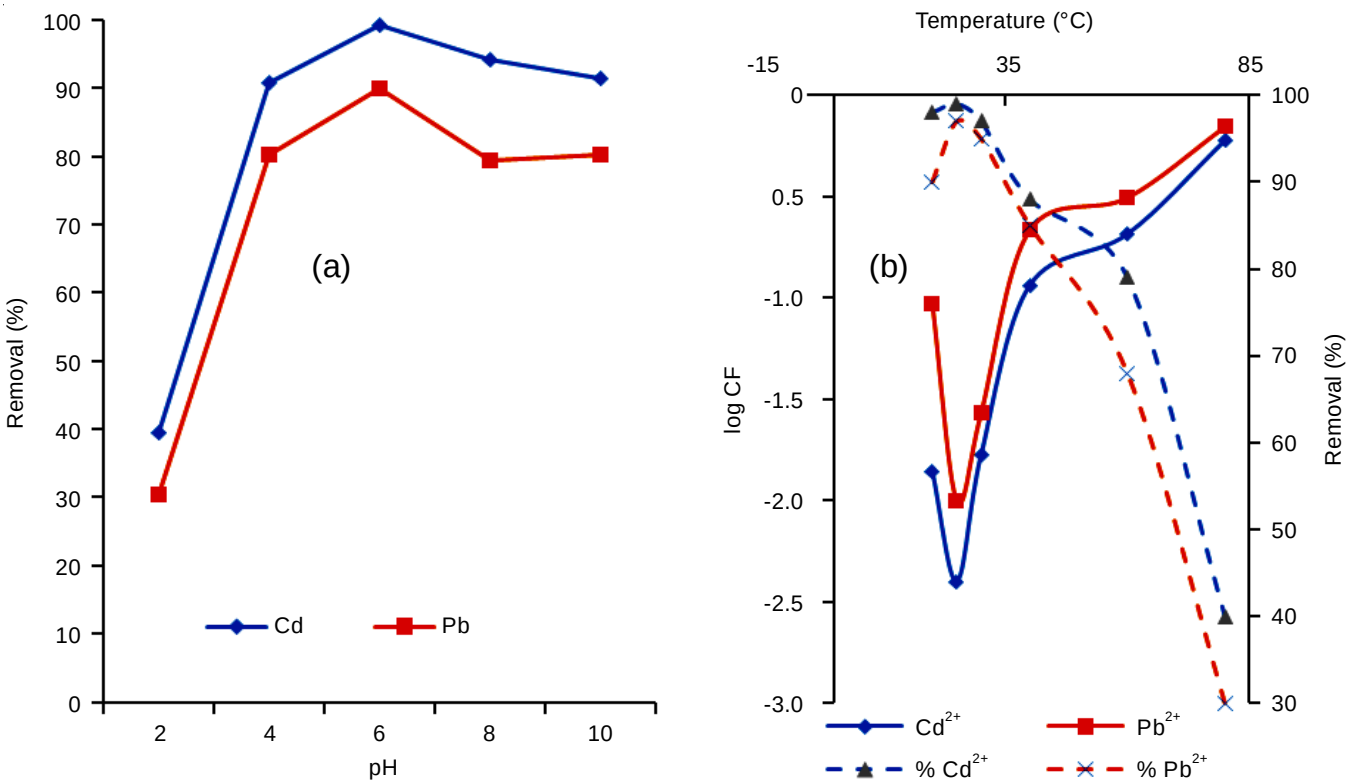

Fig. 6. Trends of Cd^{2+} and Pb^{2+} removal efficiencies with varying (a) pH and (b) temperature

Cd^{2+} and Pb^{2+}, respectively. The poor adsorption at acidic pH can be attributed to the intense competition for adsorption sites between the protons (H^+) and the heavy metal ions in solution. But as pH increases, more adsorption sites become available to the heavy metal ions, hence a sharp increase in adsorption capacity [20]. Beyond pH 6, a gradual drop in the adsorption capacity of Cd^{2+} and Pb^{2+} was observed, and this can be attributed to the increased electrostatic interaction between the heavy metal ions and the hydroxyl ions in solution.

Effect of temperature: The effect of temperature on the adsorption of Cd^{2+} and Pb^{2+} onto the prepared adsorbent (IL-AC-Fe_3O_4) was investigated in the temperature range 20 to 80 ºC. The results obtained indicated that optimum adsorption was achieved at 25 ºC, where Cd^{2+} and Pb^{2+} removal efficiencies of 99 and 97%, respectively were attained. It was observed that further increase in temperature beyond 25 ºC resulted in a rapid decrease in the adsorption of the heavy metal ions. A temperature of 25 ºC allowed rapid attainment of adsorption equilibrium and temperatures beyond that had an opposite effect, suggesting that the adsorption process using the IL-AC-Fe_3O_4 was an exothermic process. Ece *et al.* [21] also reported an exothermic adsorption in the removal efficiency of benzene and toluene using Fe_3O_4/AC@ SiO_2@1,4-DAAQ magnetic nanoparticles adsorbent as the adsorption capacity decreased with increase in temperature. This may be attributed to damage to the surface of nanoadsorbents at elevated temperatures.

Effect of contact time: The effect of contact time on the adsorption of Cd^{2+} and Pb^{2+} on IL-AC-Fe_3O_4 was investigated using different initial concentrations at 25 ºC over a period of 320 min (Fig. 7a-b). The results show increased adsorption with increasing time, with equilibrium being attained after 200 min of exposure for both Cd^{2+} and Pb^{2+}. Sahu *et al.* [22] reported similar observations in the removal of Cr^{6+} from water using Tamarind wood activated carbon.

Adsorbent dosage: To evaluate the effect of adsorbent dose on the adsorption of Cd^{2+} and Pb^{2+} using IL-AC-Fe_3O_4, the adsorbent dose was varied between 0.05 and 0.30 g (Fig. 7c). Removal efficiencies of Cd^{2+} and Pb^{2+} were observed to increase with an increase in adsorbent dose (94.9 and 90.6% with a dose of 0.05 g and, 99.9 and 99.8% with a dose of 0.30 g, respectively). An adsorbent dose of 0.15 g was established to be the optimum since very little change in adsorption removal efficiencies for Cd^{2+} and Pb^{2+} was observed beyond this dose. Adopting this value (0.15 g) as optimum adsorbent dose would allow the adsorption process to be carried out in a cost-effective manner.

Adsorption capacity: The adsorption capacity of IL-AC-Fe_3O_4 nanoadsorbent was evaluated in comparison with AC-Fe_3O_4 and Fe_3O_4 to ascertain if there was improvement in performance owing to modification with the ionic liquid (1-ethyl-3-methylimidazolium chloride). The results obtained indicated that IL-AC-Fe_3O_4 exhibited higher adsorption capacity compared to AC-Fe_3O_4 and Fe_3O_4. This improvement in performance can be attributed to the improved stability of the ionic liquid modified adsorbent (AC-Fe_3O_4). It is reported in literature that the poor performance of magnetic particles is attributed to formation of aggregates owing to magnetic dipolar attractions. This problem can be addressed by coating the surface of a magnetic adsorbent with a polymer compound [23].

Adsorption isotherms: The effects of solution concentration on Cd^{2+} and Pb^{2+} adsorption capacities were investigated

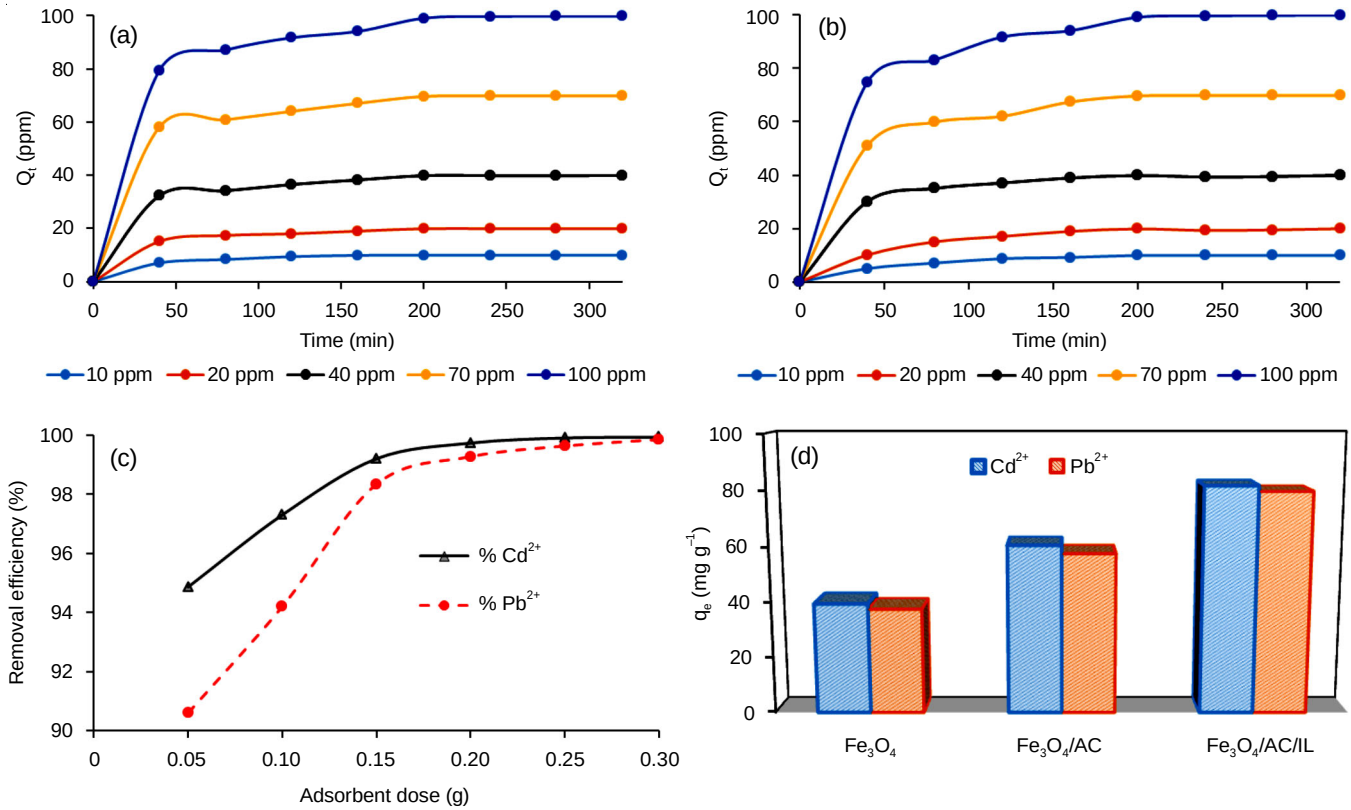

Fig. 7. Effects of contact time (a) Cd^{2+} and (b) Pb^{2+}; and (c) adsorbent dose on adsorption of Cd^{2+} & Pb^{2+} using IL-AC-Fe_3O_4 at 25 °C and pH 6; and (d) performance of IL-AC-Fe_3O_4 in comparison with AC-Fe_3O_4 and Fe_3O_4

by varying the initial concentration between 10 and 100 ppm at 25 ºC and pH of 6. Adsorption isotherms were plotted (Fig. 8) and various parameters calculated (Table-2). Comparison of the correlation coefficient values (R^2) of the two models revealed that the Freundlich model shows a better correlation than the Langmuir model meaning that the adsorption process is multilayer. The n values (parameter related to adsorption capacity and intensity of Freundlich isotherm) for the adsorption

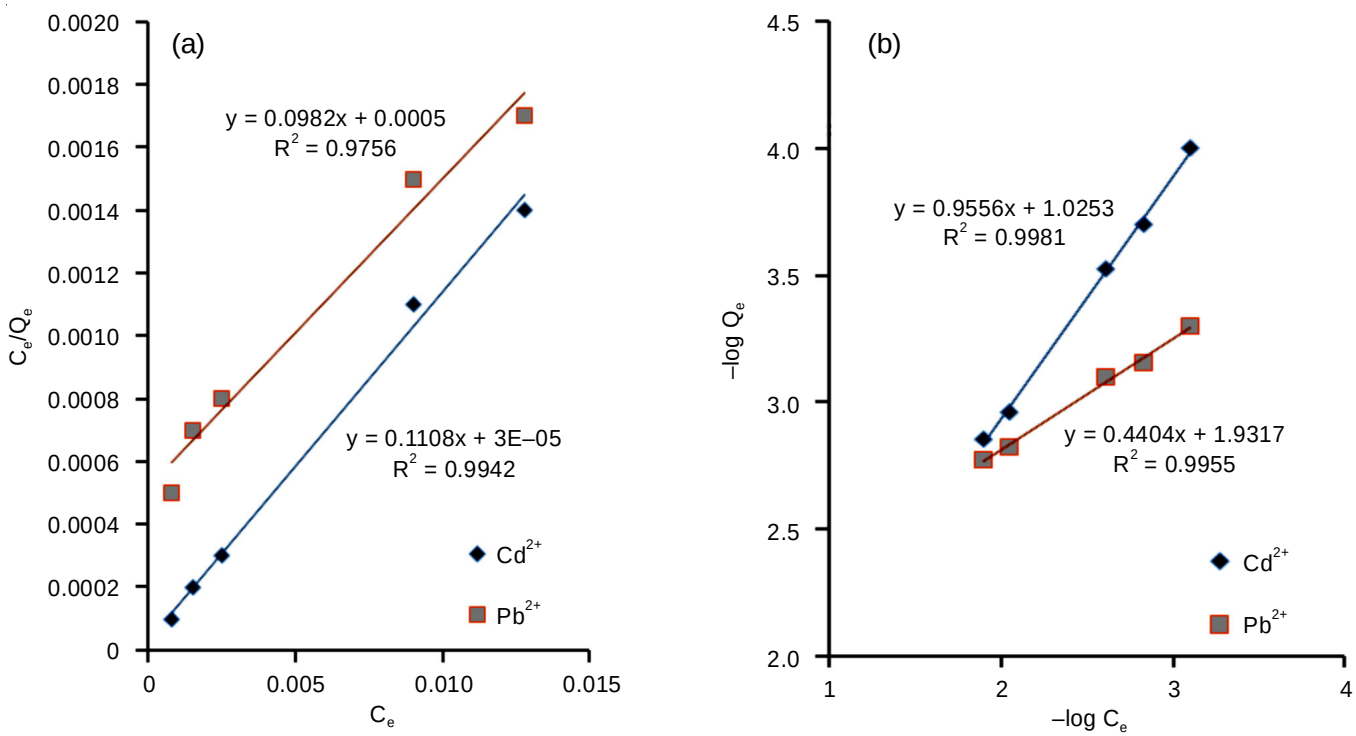

Fig. 8. Adsorption isotherms (a) Langmuir and (b) Freundlich model for adsorption of Cd^{2+} and Pb^{2+} ions on IL-AC-Fe_3O_4

TABLE-2
LANGMUIR AND FREUNDLICH ISOTHERM CONSTANTS FOR THE ADSORPTION OF Cd^{2+} AND Pb^{2+} IONS ON IL-AC-Fe_3O_4

	Langmuir isotherm				Freundlich isotherm			
	Q_e (mg/g)	b (L/mg)	R^2	R_1	K_f (mg/g)	1/n	n	R^2
Cd^{2+}	10.1833	196.4000	0.9756	0.0051	10.6000	0.9556	1.0465	0.9981
Pb^{2+}	9.0253	1107.0000	0.9942	0.0009	85.4476	0.4404	2.2706	0.9955

of both metals were greater than 1, which indicated favourable adsorption.

For understanding of the adsorption mechanism of Cd^{2+} and Pb^{2+} onto IL-AC-Fe_3O_4 nanoadsorbent, the kinetic experimental data was fitted into the pseudo first order and pseudo second order kinetic models (Fig. 9). Table-3 summarizes the adsorption kinetic model parameters obtained for the models. The R^2 values for the pseudo first-order model are close to unity and this means that the model can be used to simulate the kinetic data of the adsorption of Cd^{2+} and Pb^{2+} onto IL-AC-Fe_3O_4 nanoadsorbent.

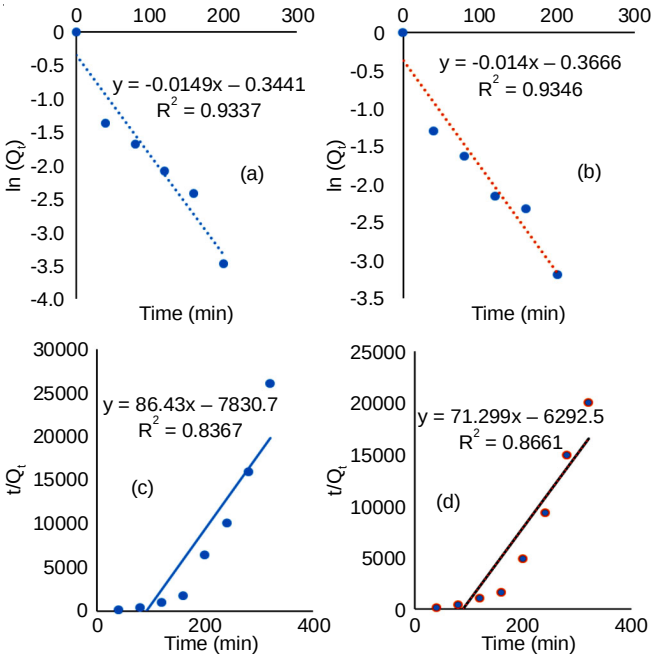

Fig. 9. Pseudo first order kinetic modelling for adsorption of (a) Cd^{2+} and (b) Pb^{2+}; pseudo second order kinetic modelling for adsorption of (c) Cd^{2+} and (d) Pb^{2+} onto IL-AC-Fe_3O_4

The calculated values of ΔHº and ΔGº are negative, which is an indication that the adsorption of Cd^{2+} and Pb^{2+} onto the IL-AC-Fe_3O_4 nanoadsorbent is an exothermic process and spontaneous (Table-4 and Fig. 10). The values were observed to decrease with increasing temperature, indicating that the adsorption process is undesirable at elevated temperatures [14]. The negative values of ΔSº, (-0.344 and -0.337 KJ mol^{-1}) for

TABLE-3
KINETIC PARAMETERS FOR ADSORPTION OF Cd^{2+} AND Pb^{2+} IONS ON IL-AC-Fe_3O_4 MNPs

Heavy metal	Pseudo first order model		Pseudo second order model	
	K_1 (min^{-1})	R^2	K_2 (g mg^{-1} min^{-1})	R^2
Cd^{2+}	0.0149	0.9337	0.00012	0.8367
Pb^{2+}	0.0140	0.9346	0.00035	0.8661

Cd^{2+} and Pb^{2+}, respectively indicated that the adsorption efficiency is independent of temperature in solid/liquid phase. The degree of entropy also decreases during the adsorption process.

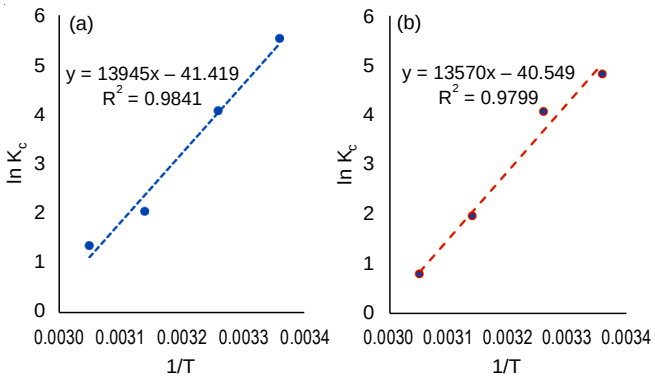

Fig. 10. van't Hoff plot for adsorption of (a) Cd^{2+} and (b) Pb^{2+} ions on IL-AC-Fe_3O_4 nanoadsorbent

Conclusion

In this study, a stable IL-AC-Fe_3O_4 magnetic nanoadsorbent was successfully prepared and evaluated in the removal of Cd^{2+} and Pb^{2+} ions from water. The findings of this study revealed that the adsorption efficiency of Cd^{2+} and Pb^{2+} ions on the magnetic nanoadsorbent was higher close to neutral pH and increased with increasing contact time and adsorbent dosage, but decreased with increasing temperature beyond 25 ºC. Modifying the magnetic nanoadsorbent with an ionic liquid improved its stability, allowing better adsorption capacity in comparison to AC-Fe_3O_4 and Fe_3O_4. The equilibrium and kinetic studies indicated that the adsorption fitted well Freundlich and pseudo first order models, respectively. Thermodynamic data showed that the adsorption of Cd^{2+} and Pb^{2+} on the IL-AC-Fe_3O_4 nanoadsorbent was spontaneous and exothermic. In this study, there is evidence that the prepared nanoadsorbent is

TABLE-4
THERMODYNAMIC PARAMETERS OF ADSORPTION OF Cd^{2+} AND Pb^{2+} ON IL-AC-Fe_3O_4

Heavy metal ions	ΔG° (Kj mol^{-1})				In K_c				ΔH° (Kj mol^{-1})	ΔS° (Kj mol^{-1})
	25 °C	35 °C	45 °C	55 °C	25 °C	35 °C	45 °C	55 °C		
Cd^{2+}	-13.67	-10.42	-5.37	-3.67	5.517	4.071	2.033	1.345	-115.94	-0.344
Pb^{2+}	-11.94	-10.42	-5.17	-2.16	4.920	4.069	1.956	0,792	-112.82	-0.337

capable of removing heavy metals ions from aqueous solutions with high efficiency owing to its large surface area and stability. The magnetic properties allow easy recovery of adsorbent after water treatment, eliminating the need for filtration, which lowers the cost of operation.

ACKNOWLEDGEMENTS

The authors acknowledge the funding from the National Research Foundation of South Africa, Grant UID: 120757.

CONFLICT OF INTEREST

The authors declare that there is no conflict of interests regarding the publication of this article.

REFERENCES

1. M. Ilyas, W. Ahmad, H. Khan, S. Yousaf, M. Yasir and A. Khan, *Rev. Environ. Health*, **34**, 171 (2019); https://doi.org/10.1515/reveh-2018-0078
2. J.M. Jacob, C. Karthik, R.G. Saratale, S.S. Kumar, D. Prabakar, K. Kadirvelu and A. Pugazhendhi, *J. Environ. Manage.*, **217**, 56 (2018); https://doi.org/10.1016/j.jenvman.2018.03.077
3. P.G. Whitehead, G. Bussi, R. Peters, M.A. Hossain, L. Softley, S. Shawal, L. Jin, C.P.N. Rampley, P. Holdship, R. Hope and G. Alabaster, *Sci. Total Environ.*, **697**, 134090 (2019); https://doi.org/10.1016/j.scitotenv.2019.134090
4. C.E. Cicero, G. Mostile, R. Vasta, V. Rapisarda, S.S. Signorelli, M. Ferrante, M. Zappia and A. Nicoletti, *Environ. Res.*, **159**, 82 (2017); https://doi.org/10.1016/j.envres.2017.07.048
5. S. Chowdhury, M.J. Mazumder, O. Al-Attas and T. Husain, *Sci. Total Environ.*, **569-570**, 476 (2016); https://doi.org/10.1016/j.scitotenv.2016.06.166
6. E. McLean, L. Fredriksen, K. Alfrey, S.R. Craig and F.T. Barrows, *Int. J. Fish. Aquat. Stud.*, **8**, 6 (2020); https://doi.org/10.22271/fish.2020.v8.i5a.2299
7. https://www.who.int/ceh/capacity/heavy_metals.pdf.
8. J. Ji, G. Chen and J. Zhao, *J. Hazard. Mater.*, **368**, 255 (2019); https://doi.org/10.1016/j.jhazmat.2019.01.035
9. X. Zhang, X. Wang, H. Qiu, D. Kong, M. Han and Y. Guo, *Colloids Surf. B Biointerfaces*, **187**, 110656 (2020); https://doi.org/10.1016/j.colsurfb.2019.110656
10. A.A.A.M. Guerra, A.F.C. Campos, R.M. de Lima, C. Kern, F.G. da Silva, G. Gomide, J. Depeyrot and A.K.B. Amorim, *J. Environ. Chem. Eng.*, **8**, 103888 (2020); https://doi.org/10.1016/j.jece.2020.103888
11. A.F.C. Campos, H.A.L. de Oliveira, F.N. da Silva, F.G. da Silva, P. Coppola, R. Aquino, A. Mezzi and J. Depeyrot, *J. Hazard. Mater.*, **362**, 82 (2019); https://doi.org/10.1016/j.jhazmat.2018.09.008
12. R.I. Rebodos and P.J. Vikesland, *Langmuir*, **26**, 16745 (2010); https://doi.org/10.1021/la102461z
13. P.L. Hariani, M. Faizal, R. Ridwan, M. Marsi and D. Setiabudidaya, *Int. J. Environ. Sci. Dev.*, **4**, 336 (2013); https://doi.org/10.7763/IJESD.2013.V4.366
14. B. Kakavandi, A. Jonidi, R. Rezaei, S. Nasseri, A. Ameri and A. Esrafily, *Iran. J. Environ. Health Sci. Eng.*, **10**, 19 (2013); https://doi.org/10.1186/1735-2746-10-19
15. S. Radi, C.E. Abiad, N.M.M. Moura, M.A.F. Faustino and M.G.P.M.S. Neves, *J. Hazard. Mater.*, **370**, 80 (2019); https://doi.org/10.1016/j.jhazmat.2017.10.058
16. Y.S. Li, J.S. Church and A.L. Woodhead, *J. Magn. Magn. Mater.*, **324**, 1543 (2012); https://doi.org/10.1016/j.jmmm.2011.11.065
17. A. Lahiri and R. Das, *Mater. Chem. Phys.*, **132**, 34 (2012); https://doi.org/10.1016/j.matchemphys.2011.10.048
18. A.H.M. Yusoff, M.N. Salimi and M.F. Jamlos, *AIP Conf. Proc.*, **1835**, 020010 (2017); https://doi.org/10.1063/1.4981832
19. S. Bandar, M. Anbia and S. Salehi, *J. Alloys Compd.*, **851**, 156822 (2020); https://doi.org/10.1016/j.jallcom.2020.156822
20. N. Tang, C.G. Niu, X.T. Li, C. Liang, H. Guo, L.S. Lin, C.W. Zheng and G.M. Zeng, *Sci. Total Environ.*, **635**, 1331 (2018); https://doi.org/10.1016/j.scitotenv.2018.04.236
21. M.S. Ece, S. Kutluay, O. Sahin and S. Horoz, *Ind. Eng. Chem. Res.*, **59**, 21106 (2020); https://doi.org/10.1021/acs.iecr.0c03883
22. J.N. Sahu, J. Acharya and B.C. Meikap, *J. Hazard. Mater.*, **172**, 818 (2009); https://doi.org/10.1016/j.jhazmat.2009.07.075
23. Renu, M. Agarwal and K. Singh, *J. Water Reuse Desalin.*, **7**, 387 (2017); https://doi.org/10.2166/wrd.2016.104